

Permeability of Macro-Fractured Sandstone Samples under Cyclic Side-Confining Pressure

W. Q. Liu^{1,2}, Y. S. Li¹, F. L. Li²

¹State Key Laboratory for Geomechanics and Deep Underground Engineering
Xuzhou 221116, China

²School of Mechanics and Civil Engineering, China University of Mining & Technology
Xuzhou 221116, China

wqliu@cumt.edu.cn; li_yushou@163.com; lflmail@163.com

Abstract - To better understand the relationship between permeability of fractured rocks and environmental confining pressure, we integrated results from experimental, analytical and numerical methods. In the experiments, we monitor the change in the permeability of fractured sandstone as confining pressure cyclically changes. The analytical models are the combination of hydro-mechanical coupling and fracture equivalence. Numerical simulation is based on the analytical models and used to further interpret the experimental measurements. We find that, 1) fracture permeability changes all by more than 50% for changes in confining pressure from 6MPa to 14MPa, 2) decreasing of fracture permeability with confining pressure has the feature of a negative exponential function, 3) pore pressure does not play an important role on seeping in fractures under high confining pressures, 4) the permeability is always lower in the second load cycle than in the first one for the same confining pressure.

Keywords: Fractured sandstone, Permeability, Cyclic confining pressure, Testing, Simulation

1. Introduction

Rock fractures conduct water more easily than pores, so revealing characteristics of fluid transport in fractures is one of significant subjects in rock hydrology. In fractures, the flow behavior or conduit permeability depends on fracture geometry. In turn, fracture geometry can be dominated by confining pressures, which are generally induced by in-situ overlying strata gravity and surrounding constraints. The chain of impacts thus leads to an indirect relationship between fracture permeability and the confining pressures.

Intact rocks usually have standard testing procedures and exhibit regular characteristics of porous flow^[1-3]. However, for fractured rocks, because of the difficulty in determining geometries and locations of fractures, seeping experiments on them still have to be constantly improved and also the testing outcome can seldom be regarded as definite one. On the basis of experimental observations, one put forward three typical models so as to theoretically simulate flow in fractured rocks. They are the equivalent-continuum model, the discrete-fractures model and the dual-porosity model^[4, 5]. In an equivalent continuum model, fractures are not independently treated but mixed into the matrix by changing matrix properties, so continuum mechanics can still work well all over the model. Modeling of discrete fractures is a meso-level treatment based on accurate investigation of location and property of each fracture. For a dual-porosity model, we must not only deal with fracture flow and pores flow separately, but also analyze the hydraulic exchange between different domains of two flows. In addition to the three models, researchers also have paid more and more attentions to the hydro-mechanically coupled response of fracture rocks, and have designed experimental or computational procedures to accurately investigate actual permeability features.

Our work in this paper was to integrate experimental, analytical and numerical methods to investigate the relationship between permeability of fractures and cyclic confining pressure. To study the impact of external pressure on fracture permeability, Davy et al. in 2007 employed transient-pressure tests for measuring water permeability of macro-cracked argillites in changing confinements^[6]. LVDT sensors surrounding a sample were used to measure fracture apertures, so their experiment had hydro-mechanically coupled analysis involved. They even introduced water-induced rock swelling for deformation superposition. Besides having totally different engineering backgrounds, our work was distinguished from Davy's mainly by the following three aspects: 1) the specimens were machined sandstones, more usual in mining

engineering; 2) the testing procedure was based on the Mechanical Testing and Simulating 815 system (hereafter MTS815) [7]; 3) the hydro-mechanically coupled analysis began from a set of coupling equations, on the equivalent-continuum platform.

2. Experimental Fractures Permeability in Cyclic Confining Pressures

The MTS815 system shown in Fig.1 is used in our experiment as a platform of loading and seeping. Sandstone samples employed here were collected from the strata of about-300m in Huainan-Guqiao mine. They were machined into 50×100mm cylinders, and then went to undergo uniaxial compression until occurring of macroscopic cracks (strength of around 30MPa, see Fig. 2). After that, the fractured specimens must be saturated with water and laterally sealed in PVC bands and thermo-shrinking plastic sleeves. Figure 3 is the detailed scheme of loading and seeping. In experiments, the axial load is a constant value of 14MPa, less than half of the uniaxial strength for fixing specimens directly from top and bottom, whereas the side confining pressure is produced by hydraulic oil and is a controllable cyclic change between 6MPa and 14MPa.



Fig. 1: The MTS815 system of loading and seeping with a sample fixed on the testing platform.



Fig. 2: The 1# sandstone sample with a through-going fracture from top to bottom.

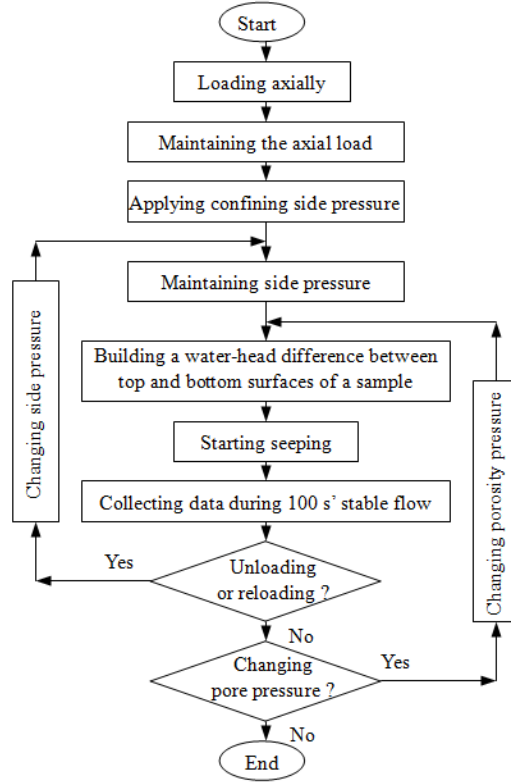


Fig. 3: Testing scheme of water seeping of fractured rock samples under cyclic confining pressures.

Testing permeability in our experiments is by the transient-pressure method. Data to be collected include top-bottom pressure difference of a sample, seepage gauging time, water flux, sample geometry, etc. Permeability then may be calculated by Eq. (1), according to the MTS815 technical handbook (<http://www.mts.com>).

$$k = \mu\beta V \left(\frac{\ln\left(\frac{\Delta p_i}{\Delta p_f}\right)}{2\Delta t\left(\frac{A_s}{L_s}\right)} \right) \quad (1)$$

where, μ is kinematic viscosity of water, β is compression coefficient, V is volume of water tank, $\Delta p_i / \Delta p_f$ is ratio of initial and final pressure differences between the top and bottom of a sample, Δt is time span between Δp_i and Δp_f with ≥ 100 s suggested here for stable testing, A_s and L_s are respectively cross-section area and length of a specimen.

Table 1 shows the testing results of permeability for three samples with different pore pressures. Figure 4 is the changing of permeability for Sample 1# under cyclic confining pressures. Figure 5 is the changing of permeability with the porous water pressure. It may be found in Table 1 that: Permeability goes down as confining pressure increases, or

Table 1: Permeabilitis of #1 /#2 /#3 fractured samples measured in cyclic side pressures $/\times 10^{-6}$ Darcy.

Side pressure /MPa	Pore water pressure /MPa		
	2.0	4.0	6.0
6.0	0.9820/14.2446/129.7077	2.0318/4.5294/148.0166	10.6826/3.8964/49.0783
8.0	0.6377/7.6432/123.2012	1.0536/0.5752/64.7563	0.9423/0.2705/0.2379
10.0	0.4653/5.9379/112.2062	0.6385/0.0691/22.6981	0.4034/0.1784/2.5968
12.0	0.2977/4.1791/94.7610	0.3704/0.1242/13.0460	0.2166/0.1340/0.1959
14.0	0.2543/3.5673/55.5263	0.2898/0.4563/5.3415	—/0.5027/0.2136
12.0	0.4440/4.4562/54.6307	0.5111/0.3744/4.8750	—/0.6870/0.8438
10.0	0.5309/4.4805/67.6648	0.6190/0.9226/1.4973	0.9111/0.8473/3.8902
8.0	0.6222/4.3473/55.7796	0.7989/0.9757/6.4684	0.9463/1.5085/9.7580
6.0	0.6955/4.1898/67.3836	1.4776/1.8488/16.4687	6.5820/2.5064/52.9601
8.0	0.4617/2.3770/33.4239	0.5874/0.1336/0.3309	0.3385/0.4382/1.3438
10.0	0.3388/1.3300/29.0354	0.3805/0.5913/1.3588	0.2295/0.0422/1.7201
12.0	0.2986/0.6232/18.3835	0.2429/0.4418/2.0808	—/0.0436/1.7249
14.0	0.2805/0.1487/15.9927	0.1736/0.5198/0.4371	—/0.4787/1.3537
12.0	0.3431/0.6240/15.7264	0.5253/0.4563/1.0148	—/0.3384/1.0404
10.0	0.4587/0.7001/16.9722	0.5377/0.6860/3.0000	—/0.9871/3.0482
8.0	0.4794/—/14.2395	0.8571/—/5.1514	1.0900/—/6.7742
6.0	0.5802/—/17.0496	1.3170/—/13.5908	6.1734/—/8.9055

Note: dashes occurring here due to data missing

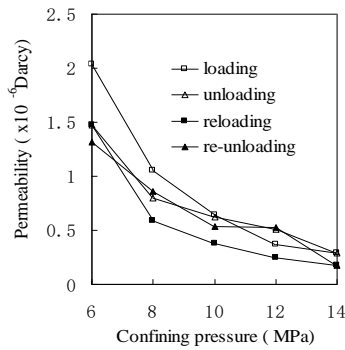


Fig. 4: Experimental permeabilities of Fractured Sample 1# with the pore pressure of 4MPa under cyclic confining pressures.

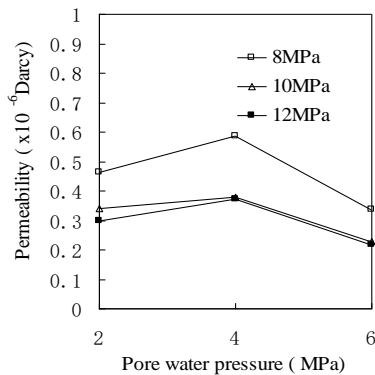


Fig. 5: Permeability-pore pressure relations for Fractured Sample 1# with confining pressures 8MPa, 10MPa and 12MPa.

contrarily unloading of pressure leads to growing of permeability; Fracture permeability changes all by more than 50% or mostly by more than 70% for changes in confining pressure from 6MPa to 14MPa; For all three samples, permeability, at the same confining pressure, is always lower in the second load cycle than in the first one (also see Fig.4). One of probable reasons is that alternating of loading and unloading leads to “plastic deformation” (change of fracture surface roughness and debris generation) and thereby makes narrowing or even clogging of fracture conduits. On the other hand, pore water pressures do not play a monotonic role on the change of permeability, compared with confining pressures, especially in the second loading-unloading cycle or in higher confining pressures (also see Fig.5). Such findings do not support the common sense that increasing pore pressure favors elevating permeability. We thought, dropping of permeability due to “plastic deformation” during load cycles still may account for the uncommon display, since varying of pore pressure is applied following alternating of load. Anyway, fracture surface reconstruction and debris distribution are indefinite to some extent and hence may produce two different directions of permeability evolution.

It also may be found in Fig. 4 that the first load cycle has 27% loss of permeability from start to finish, but the second cycle has only 11% loss, less than half of the first one. The obvious difference of permeability loss should mainly be attributed to “plastic deformation” of fractures. Moreover, permeability change in each loading or unloading segment may be fitted very well with an exponential curve ($R^2=0.9801, 0.9607, 0.9585$ or 0.9010 in sequence for each monotonic load changing). In the first step of loading or the last step of unloading, permeability changes more dramatically than in any other load steps.

3. The Fluid-Solid Coupling Model and Its Numerical Solution

Note the effective stress as

$$\sigma_{ij}' = \sigma_{ij} - zp\delta_{ij} \quad (2)$$

where, σ_{ij}' and σ_{ij} are the effective stress and the general stress, respectively; $z=1-B_0/B_s$ is the constant fracture-related factor, in which B_0 and B_s are effective and matrix bulk moduli, respectively; p is the fluid pressure; δ_{ij} is Kronecker’s delta. By combining the equation of fluid continuity with the equation of solid equilibrium, we may produce a coupling model

$$\begin{cases} \frac{\partial}{\partial x_i} \left(\frac{K_{ij}}{\rho g} \frac{\partial p}{\partial x_j} \right) - \frac{\partial}{\partial x_i} \left(\frac{\partial u_i}{\partial t} \right) = 0 \\ (\lambda + G)\nabla \cdot (\nabla u_i) + G\nabla^2 u_i + F_i - z\nabla p = 0 \end{cases} \quad (3)$$

where K_{ij} is the seepage coefficient tensor; u_i is the displacements of fracture surfaces; G and λ are the shearing modulus and Lamé’s constant of the matrix; F_i is the body force. Since this model has considered the role of fractures on seeping, it completely may simulate our experimental problem. The following is the numerical calculation of this model based on the software COMSOL (<http://www.comsol.com>).

In calculation, we have a simplification from 3D to 2D, no distinguishing between two transverse directions. The model was taken according to the size of experimental samples, 100 mm in length and 50 mm wide. The top and bottom boundaries have no displacements. The model has side pressures from 6 ~ 14 MPa at 2 MPa increments. Its Young’s modulus is 100 GPa and Poisson’s ratio is 0.25, suggested from the average of experimental samples. The fluid pressure difference between top and bottom surfaces is 0.3MPa, while the averaged pore pressure is 4MPa. In addition, permeability changes in exponent laws as side pressure is unloaded. The model was meshed into 200 Lagrange-Quadratic elements with 2583 degrees of freedom.

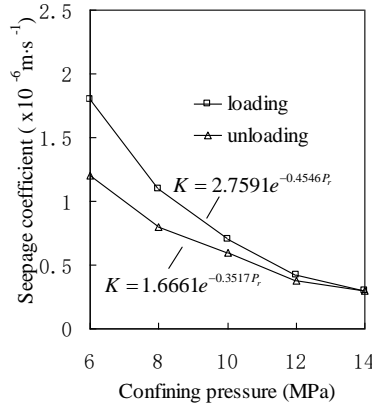


Fig. 6: The relation between seepage coefficient and confining pressure used in numerical simulation.

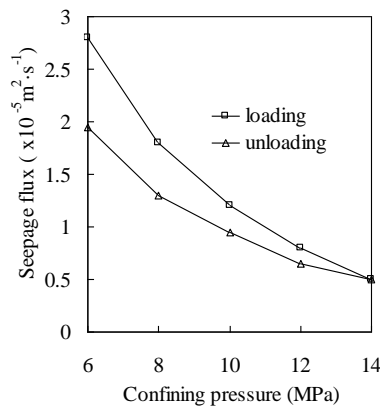


Fig. 7: The negative exponential relation of seeping flux with confining pressure produced by numerical calculation.

The fracture factor “z” can be chosen carefully according to experimental testing and the definition calculation. For simplicity, we took the widely accepted value for engineering problems, 0.4, as the coupling coefficient of fractures. In addition, we also change the confining pressures from 6 ~ 14 MPa and then from 14 ~ 6 MPa at 2 MPa increments. The permeability, similar to the experimental results, is approximately the negative exponential function of confining pressure. Figure 6 shows the permeability-pressure exponential curves and corresponding fitting relations, respectively for loading and unloading. In this figure, we set the beginning of unloading right at the end of loading, and the value of permeability at the unloading end is 70% of the value at the loading start.

With the model of Eq. (3), $z=0.4$ and the permeability relations of Fig.6, we can then calculate with the COMSOL and produce the seeping flux as shown in Figs. 7. In order to simplifying the calculation, we assumed that the element has the same coupling relations of permeability-pressure as the entire model. It may be found from Fig. 7 that the pressure-dependent relation of seeping flux also has an exponential-function feature. The flow flux increases if the confining pressure goes down, or the flow flux decreases if the confining pressure goes up. The exponential-function feature of flow flux is mainly because of meeting the Darcy law, i.e. the flux is directly proportional to the permeability under the condition of a constant pressure difference

4. Conclusion

We completed a group of experiments with MTS815 for investigating the impact of cyclic loading on the permeability of fractured sandstone. Also, we built a coupling model of seeping in fractures and numerically simulated the flow in fractured media. The fracture-related factor is optimally-selected and used in modeling and simulating. By testing and simulating, we have the following conclusions:

1) Cyclic loading has significant impact on the permeability of fractured rock, while pore pressure does not play an important role on seeping in fractures. A negative exponential relation exists between confining pressure and permeability, and going-up of confining pressure leads to going-down of permeability.

2) At the same confining pressure, the permeability is always lower in the second load cycle than in the first one. Furthermore, the first cycle has a bigger permeability difference, between the loading start and the unloading end, than the second cycle, 27% vs 11% for our experiments.

3) The optimal fracture-related factor is a critical value dominating the transformation of pressure-length curves, 0.4 for our coupling model of simulating seeping in fractured rock. The seeping flux of fractured rock also may have negative exponential relations with confining pressure.

Acknowledgements

The authors thank Prof. M. Manga at UC Berkeley for comments. This study was supported by Special Subject Grant of National “973” Basic Research Program of China (No. 2015CB251602 and No.2009CB219605), National Natural Science Foundation of China (No. 41074040 and No. 50774083), Jiangsu Natural Science Foundation (No. BK20141125) and Chinese Program for New Century Excellent Talents in University (No. NCET-07-0803).

References

- [1] Y. G. Gong and Y. D. Xie, “A review of laboratory investigation of rock permeability,” *Chin. J Rock Mech. Eng.*, vol. 8, no. 3, pp. 219-227, 1989.
- [2] J. Bear and Y. Bachmat, *Introduction to modeling of transport phenomena in porous media*. Norwell MA: Kluwer, 1990.
- [3] F. Homand, A. Giraud, S. Escoffier, et al, “Permeability determination of a deep argillite in saturated and partially saturated conditions,” *Int. J Heat Mass Transfer*, vol. 47, no. 14, pp. 3517-3531, 2004.
- [4] F. Thauvin and K. K. Mohanty, “Network modeling of non-Darcy flow through porous media,” *Transport in Porous Media*, vol. 31, no. 1, pp. 19-37, 1998.
- [5] W. Q. Liu, X. X. Miao and Z. Q. Chen, *Seepage Theory of Mining Strata*. Beijing: Science Press, 2004.
- [6] C. A. Davy, F. Skoczylas, J. D. Barnichon, et al, “Permeability of macro-cracked argillite under confinement: Gas and water testing,” *Phys. & Chem. Earth*, vol. 32, no. 8, pp. 667-680, 2007.
- [7] S. P. Li, D. X. Wu, W. H. Xie, et al, “Effect of confining pressure, pore pressure and specimen dimension on permeability of Yin Zhuang sandstone,” *Int. J Rock Mech. Min. Sci.*, vol. 34, no. 3-4, pp. 435-441, 1997.